Numerical modeling of natural convection induced by a heated chip in a square cavity containing an adiabatic obstacle and a hybrid nanofluid Fe_3O_4- Al_2O_3/water

Mohsine Qaffou[1,], Youness Ighris[1], Yassine Bouhouchi[1], Meryem Maiss[1], Ahmed Moussaoui[2], Jamal Baliti[1], and Mohamed Hssikou[1]*

[1] Research team in Smart Electrical, Mechanical and Energy Systems (SEMES), Polydisciplinary Faculty, Sultan Moulay Slimane University, Beni Mellal, Morocco
[2] Faculty of Sciences, Moulay Ismail University, Meknes, Morocco

Abstract. In this work, we propose a numerical study of two-dimensional natural convection in a closed square enclosure that encloses an adiabatic square block and contains the hybrid nanofluid Fe_3O_4-Al_2O_3/water. The cavity's two horizontal walls are thought to be adiabatic, while its two vertical walls are arranged so that the right wall is totally cold and the left wall is heated by a chip with a width of l = L/2. The average Nusselt number along the cold wall, streamlines, and isotherms are used to report the results. The findings show that fluid flow and heat transfer in the cavity are strongly influenced by the location of the heated chip. The chip's central location produces the most effective heat exchange, while Rayleigh intensification improves convection and raises the average Nusselt number on the cold wall. This arrangement greatly enhances heat transfer inside the cavity and optimizes the distribution of current lines. *Corresponding author:

1. Introduction

Over the past several years, numerous studies have focused on heat transfer within cavities that have walls heated differentially. Natural convection is a particularly attractive mode of heat transfer in many industrial applications. Indeed, a large number of studies of square, rectangular, triangular, and inclined cavities with different boundary conditions have been intensively considered by researchers [1]-[2]. Improvements in heat transfer in cavities through the introduction of blocks in the walls have been extensively studied in recent years [3]-[4] Research in this field covers a very broad area because the applications involved are extremely varied. Rajarajeswari et al. [5] conducted a numerical investigation of natural convection within a square cavity featuring an inclined prismatic obstacle, utilizing Comsol software for their analysis. The influence of Ra and the orientation of the obstacle on flow fields, isotherms, and heat transfer was analyzed. In addition, machine learning methods were

*Corresponding author: mohsine.qaffou@usms.ac.ma

implemented to optimize the thermal performance of the system. Garoosi [6] analyzed natural convection in a square cavity containing a square cooler using a hybrid SPH–MPS model based on a Lagrangian particle approach. The numerical model was validated using several test cases, demonstrating its robustness in reducing pressure instabilities and limiting particle-induced turbulence. The results confirm that this model can reliably simulate heat transfer in complex configurations, including a cavity with a cold internal obstacle. Al Srayyih et al. [7] investigated the influence of two oscillating elliptical obstacles on natural convection heat transfer and entropy generation in a quarter-circular cavity filled with a Cu - Al_2O_3 hybrid nanofluid. The results show that lengthening the heated wall reduces heat transfer, while increasing the Rayleigh number significantly increases total entropy and irreversibility. The amplitude of the oscillations has a greater influence on Nu_{av} than their frequency, with behavior that depends on whether the Rayleigh number is low or high. Ouallal et al. [8] proposed LBM to simulate the flow of an Oldroyd-B type viscoelastic fluid around square and circular obstacles in a cavity. This model allows analysis of flow structure, vortex formation, and the influence of parameters such as Reynolds and Weissenberg numbers, as well as the size, shape, and position of obstacles. The results obtained in steady-state and transient conditions highlight the significant impact of these parameters on internal flow mechanisms.

This work focuses on the numerical study of natural convection developing in a square cavity containing an adiabatic obstacle placed at its center, whose length is half that of the cavity. The left vertical wall is subjected to localized heating by a thermal chip that can occupy three positions (bottom, midlle, top), while the right vertical wall is kept completely cold. The horizontal walls are considered adiabatic. The objective is to investigate the effects of the main control parameter, particularly the Rayleigh number, together with the heating source location, on the flow patterns and heat transfer performance inside the cavity. The results obtained can thus contribute to optimizing the positioning of dissipative components in electronic systems, with a view to improving their reliability and service life.

2. Mathematical Description of the Problem

2.1 Problem Formulation

The physical model investigated in the present study is depicted in Fig. 1. The system consists of a square cavity of characteristic length L, filled with a Fe_3O_4-Al_2O_3/water hybrid nanofluid at a solid volume fraction of $\phi = 0.06$. The cavity contains a square adiabatic obstacle with width $l = 0.5 \times L$ at its center. The right vertical wall is maintained at a constant cold temperature T_C, while the left vertical wall is partially heated by a thermal chip heated to T_H; the remaining portion of this wall is considered adiabatic. The horizontal walls are also assumed to be thermally insulated. The heat source can be placed in three different positions on the left vertical wall : at the bottom, in the center, or at the top. The thermal gradient imposed by the chip induces convective motion, which causes energy to be transported to the cold wall. All thermo-physical properties of the fluid are considered constant, except for the density in the buoyancy term, where the Boussinesq approximation is applied. Thermal radiation effects are disregarded, and the hybrid nanofluid is treated as a Newtonian, incompressible fluid undergoing laminar flow.

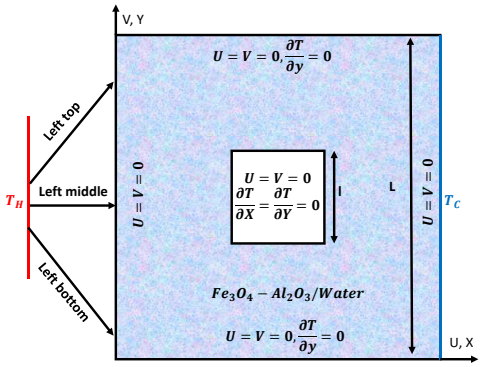

Fig.1. studied geometry

Table 1 summarizes the thermo-physical characteristics of the base fluid and the considered nanoparticles.

Table 1. Thermophysical characteristics of the base fluid and nanoparticles. [9]-[10]

Physical characteristics	Water	Fe_3O_4	Al_2O_3
$\rho(Kg/m^3)$	997.1	5200	3970
$C_P(J/Kg.K)$	4179	670	765
$\lambda(W/m.K)$	0.613	6	25
$\beta.10^{-5}(1/K)$	21	1.3	0.85
P_r	6.2	-	-

Equations (1-4) represent the thermo-physical characteristics of the hybrid nanofluid, such as its density (ρ_{hnf}), heat capacity ($C_{P_{hnf}}$), coefficient of thermal expansion (β_{hnf}), and thermal diffusivity (α_{hnf}).

$$\rho_{hnf} = (1-\phi).\rho_f + \phi_{Al_2O_3}.\rho_{Al_2O_3} + \phi_{Fe_3O_4}.\rho_{Fe_3O_4}, \quad (1)$$

$$(\rho.C_P)_{hnf} = (1-\phi).(\rho.C_P)_f + \phi_{Al_2O_3}.(\rho.C_P)_{Al_2O_3} + \phi_{Fe_3O_4}.(\rho.C_P)_{Fe_3O_4}, \quad (2)$$

$$(\rho.\beta)_{hnf} = (1-\phi)(\rho\beta)_f + \phi_{Al_2O_3}(\rho\beta)_{Al_2O_3} + \phi_{Fe_3O_4}(\rho\beta)_{Fe_3O_4}, \quad (3)$$

$$\alpha_{hnf} = \frac{\lambda_{hnf}}{(\rho C_P)_{hnf}}. \quad (4)$$

Where ϕ indicates the solid volume fraction $\left(\phi = \phi_{Al_2O_3} + \phi_{Fe_3O_4}\right)$.

The thermal conductivity of hybrid-nanofluid (λ_{hnf}) is calculated as follows :

$$\lambda_{nf} = \lambda_f \frac{\lambda_{Al_2O_3} + 2\lambda_f - 2\phi_{Al_2O_3}\left(\lambda_f - \lambda_{Al_2O_3}\right)}{\lambda_{Al_2O_3} + 2\lambda_f + \phi_{Al_2O_3}\left(\lambda_f - \lambda_{Al_2O_3}\right)}, \quad (5)$$

$$\lambda_{hnf} = \lambda_{nf} \frac{\lambda_{Fe_3O_4} + 2\lambda_{nf} - 2\phi_{Fe_3O_4}\left(\lambda_{nf} - \lambda_{Fe_3O_4}\right)}{\lambda_{Fe_3O_4} + 2\lambda_{nf} + \phi_{Fe_3O_4}\left(\lambda_{nf} - \lambda_{Fe_3O_4}\right)}. \quad (6)$$

The viscosity of the nanofluid (μ_{hnf}) :

$$\mu_{hnf} = \frac{\mu_f}{(1-\phi)^{2.5}}. \quad (7)$$

The subscripts f and hnf denote the base fluid and the hybrid nanofluid, respectively.

By applying these assumptions within the Boltzmann framework, the dimensionless governing equations for the density and temperature distribution functions can be written as follows [11]:

$$f_k(x_k + c_k \Delta t, t+\Delta t) = (1-\omega_f).f_k(x_k, t) + \omega_f.f_k^{eq}(x_k, t) + F_{b,k}, \quad (8)$$

$$g_k(x_k + c_k \Delta t, t+\Delta t) = (1-\omega_g).g_k(x_k, t) + \omega_g g_k^{eq}(x_k, t). \quad (9)$$

where $\omega_f = \frac{1}{\tau_f}$, $\tau_g = \frac{1}{\omega_g}$, and $F_{b,k}$, represent the collision frequency, thermal relaxation time, and driving force per unit mass in the k-direction, respectively.

$$F_{b,k} = 3\,\omega_k c_k \rho g \beta (T - T_{ref}). \quad (10)$$

Here, $T_{ref} = (T_h + T_c)/2$, denotes the reference temperature, where β denotes the thermal expansion coefficient, while g represents the gravitational acceleration.

The dimensionless parameters governing the present problem are defined as follows:

$$\theta = \frac{T - T_C}{T_H - T_C}, (X,Y) = \frac{(x,y)}{H}, (U,V) = \frac{(u,v)}{\sqrt{g.\beta_{hnf}.(T_H - T_C).H}}. \quad (11)$$

The governing dimensionless parameters are expressed as follows:

$$Ra = \frac{g_r \beta_f L^3 (T_H - T_C)}{\nu_f \alpha_f}, Nu_r = -\frac{\lambda_{hnf}}{\lambda_f}\left.\frac{\partial \theta}{\partial X}\right|_{X=1}, Nu_{avr} = /\int_0^1 Nu_r.dY\ /. \quad (12)$$

Where Ra, Nu_r, and Nu_{avr} denote the Rayleigh number, the local Nusselt number along the right wall, and the corresponding average Nusselt number, respectively.

The macroscopic quantities are evaluated as follows:

$$\rho = \sum_{k=0}^{8} f_k, U = \frac{1}{\rho}\sum_{k=0}^{8} f_k c_k, \theta = \sum_{k=0}^{8} g_k. \quad (13)$$

2.2 Results and analyses

This article employs a numerical approach using LBM, implemented in Fortran, to investigate free convection inside a square cavity containing an adiabatic obstacle and filled with the hybrid nanofluid Fe_3O_4-Al_2O_3/water. Heat transfer management is examined by modifying the position of the heating source placed on the vertical left wall. First, a sensitivity study on mesh size is performed to evaluate numerical accuracy, followed by model validation. A detailed analysis of the influence of the main simulation parameters is then carried out to characterize the flow and thermal performance of the system.

2.2.1 Mesh stabilization

To guarantee that the numerical results are not affected by spatial discretization, a mesh independence analysis was performed. The average Nusselt number (Nu_{av}) on the hot wall and the minimum absolute value of the streamline ($|\psi_{min}|$) were calculated for various mesh resolutions, with the Rayleigh number set at Ra = 10^5. The results show that refining the mesh gradually reduces the differences between solutions, confirming numerical convergence. On this basis, a 180×180 node grid was adopted for all simulations, offering an optimal compromise between accuracy and computational cost.

Table 2. Nu_{av} and $|\psi_{min}|$ values for different mesh sizes.

	90	110	150	180	210
$\boldsymbol{Nu_{av}}$	4.718	4.721	4.724	4.732	4.748
$\boldsymbol{\lvert\psi_{min}\rvert}$	10.954	10.974	10.983	10.983	10.984

2.2.2 Numerical Model Validation

The numerical code developed in Fortran was validated by comparing its results with those reported by B. Ghasemi[12] for natural convection in a square cavity filled with an Al_2O_3/water. In that setup, the left vertical wall is kept at a high temperature, the right vertical wall at a lower temperature, and the horizontal walls are considered adiabatic. The average Nusselt number values on the heated wall, as well as the maximum current lines, reported in Table 3, constituted the validation criteria. In addition, the code adapted for this study was also validated by simulating a classic case of a fully heated cavity, and the results obtained were compared with experimental data collected by Krane and Jessee[13], as illustrated in Fig 2. The discrepancies between numerical and experimental results remain small, confirming the validity and reliability of the numerical simulation in relation to the data available in the literature.

Table 3. Nu_{av} and Ψ_{max} values for ϕ at $Ra = 10^5$.

	$\boldsymbol{\phi}$	0.0	0.02	0.04	0.06
Ghasemi	Nu_{av}	4.738	4.820	4.896	4.968
	Ψ_{max}	11.053	11.313	11.561	11.801
Present results	Nu_{av}	4.721	4.816	4.903	4.982
	Ψ_{max}	10.987	11.240	11.487	11.732

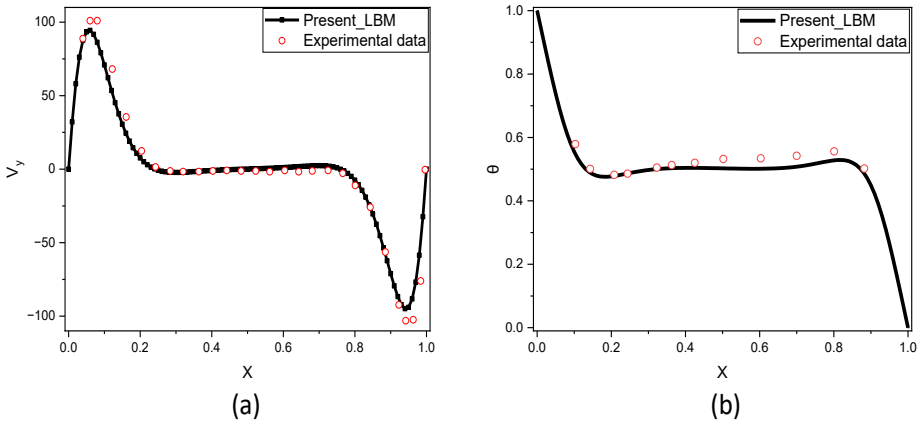

Fig. 2. Comparison of the present numerical results with previous studies for air confined in a square enclosure at Ra = $1.89.10^5$.

2.2.3 Influence of Rayleigh Number and Heating Chip Position

In this section, the interaction between Ra and the position of the localized heating is analyzed based on the isotherms, streamlines, and vertical velocity profiles shown in Fig. 3-5, as well as the average Nusselt number reported in Table 4. The Rayleigh number is considered over the interval $10^3 \leq \text{Ra} \leq 10^6$. The heating chip is placed in three different positions, as shown in Fig. 1.

According to Fig. 3, the isotherms obtained show that the thermal behavior of the cavity depends heavily on Ra and the position of the heating chip. For $Ra = 10^3$, the isotherms are almost parallel, indicating a predominantly conductive heat transfer regime. In this case, the position of the chip causes only slight deformations around the obstacle, confirming that buoyancy is insufficient to significantly disrupt the thermal distribution. When $Ra = 5.10^4$, convection becomes more pronounced and the isotherms tend to align horizontally, reflecting the gradual transition to convection-dominated heat transfer. The structure of the isotherms also varies depending on the position of the chip. A chip placed at the left bottom position induces a gradual rise of hot fluid along the wall, while a left midlle position position generates a more symmetrical thermal distribution around the obstacle. Conversely, heating at the left top creates a high thermal gradient in the upper region, revealing a direct interaction between the rising fluid and the ceiling of the cavity. For $Ra = 10^6$, the thermal field is strongly distorted by the dominant convection. The isotherms align horizontally and converge sharply near the chip and around the obstacle. The chip placed at the left top causes significant distortion of the thermal field, with a very thin thermal boundary layer and strongly compressed isotherms in the upper region, reflecting intensified heat transfer. This configuration generates the highest thermal gradients, confirming that the upper position of the chip is the most thermally dynamic.

As shown in Fig. 4, the streamlines predominantly move downward along the cold wall, indicating that the fluid flows clockwise. The structure and intensity of the streamlines depend heavily on the convective force, imposed by Ra, as well as on the vertical position of the heating chip. For $\text{R}a = 10^3$, the flow remains dominated by conduction. A single convection cell occupies the entire cavity, and the position of the chip induces only slight deformations, indicating that buoyancy is insufficient to disrupt the main circulation. The intensity of the streamlines remains low, with a slight influence from the position of the chip : the left midlle position corresponds to the maximum intensity ($|\psi_{min}| = 0.638$), followed

by the left bottom position ($|\psi_{min}| = 0.612$) and finally the left top position ($|\psi_{min}| = 0.528$). At $Ra = 5 \times 10^4$, convection becomes significant and the position of the chip modifies the topology of the flow lines. The left midlle position promotes symmetrical circulation, while a chip placed at the top causes the formation of a secondary vortex due to increased shear. The intensity of the flow increases overall and depends on the position of the chip : the left bottom position generates the most intense flow ($|\psi_{min}| = 8.038$), followed by the left midlle position ($|\psi_{min}| = 6.826$), while the left top position has the weakest flow ($|\psi_{min}| = 4.615$), indicating that this configuration remains less favorable for the development of the flow. For $Ra = 10^6$, convection is dominant and the streamlines occupy a large part of the cavity. In all three configurations, well-defined secondary vortices appear around the obstacle, but their intensity and location depend heavily on the position of the heating chip. When the chip is placed at the left top position, the fluid quickly reaches the ceiling, causing the jet to separate and a large recirculation zone to form in the upper right-hand corner. This configuration thus has the greatest disruptive effect on the flow structure.

According to Fig. 5, for Ra = 10^3, the profiles associated with the three positions of the chip are almost identical, reflecting a regime in which natural convection remains weak. At this Rayleigh number, heat transfer is mainly governed by conduction, and the flow remains weak, leading to velocity profiles with little contrast. When Ra reaches 5. 10^4, the curves clearly separate depending on the position of the hot source. The intensification of buoyancy forces promotes the establishment of more pronounced convective structures, particularly near thermally active areas. The chip at the bottom produces the highest speeds, followed by chip in the center, while the chip at the top position shows a more attenuated response, indicating increased sensitivity of the flow dynamics to the location of the heating. Finally, for Ra = 10^6, convection is fully developed and the differences between profiles become very pronounced. The chip at the bottom leads to a marked acceleration of the fluid, revealing more vigorous updrafts and more intense recirculation in the cavity. At this regime, the velocity distribution becomes highly non-uniform, confirming the decisive influence of Ra and the position of the hot source on the flow structure.

The variation of the average Nusselt number along the cold right wall, reported in Table 4 for different heating chip locations and Rayleigh numbers, indicates a marked enhancement of Nu_{avr} as Ra increases. This reflects the amplification of thermal gradients and the reduction in the thickness of the thermal boundary layer when convection becomes dominant. The study shows that the left midlle position of the chip systematically leads to the most efficient heat transfer, with maximum values for the average Nusselt number. This performance can be explained by more optimal interaction between the heated area and the cold wall, which helps to reinforce the overall thermal gradient. In contrast, the left bottom and left top positions offer more modest performance. When the chip is placed in the left bottom position, the natural rise of the hot fluid limits the impact on the cold wall, while in the left top position, heat accumulation in the upper area reduces thermal gradients. Thus, the central position of the chip appears to be the optimal configuration for maximizing thermo-fluidic exchanges within the cavity.

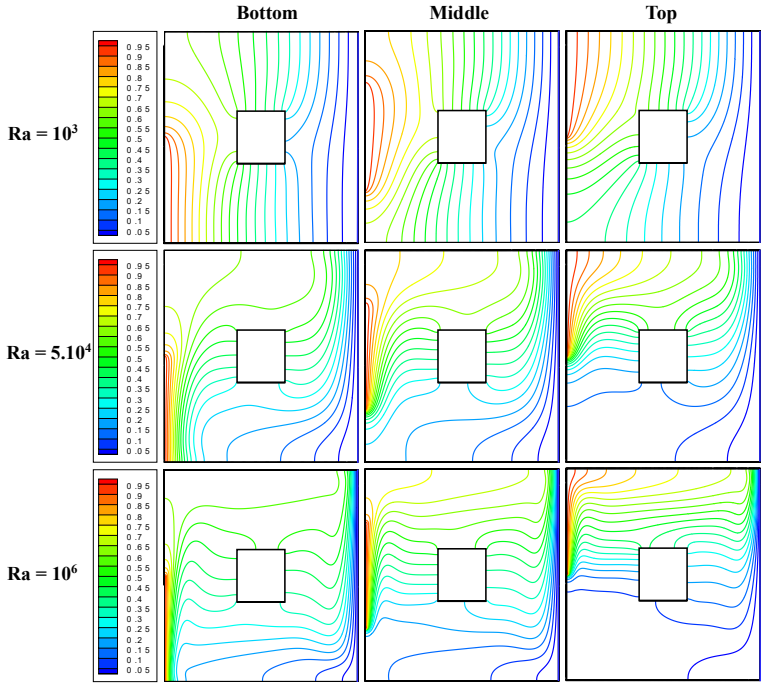

Fig. 3. Distributions for various heating chip positions at three different Ra values.

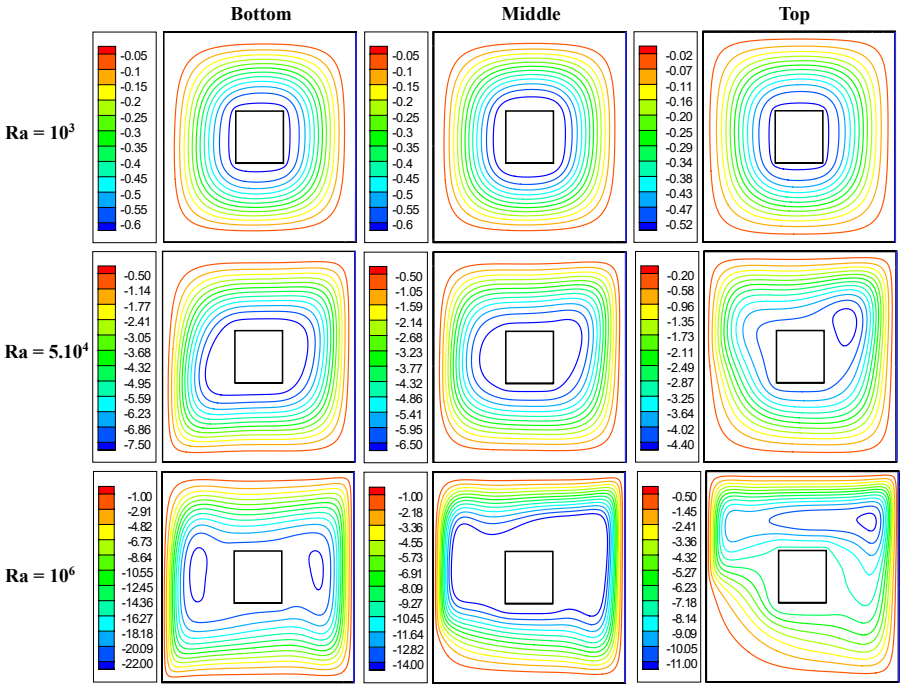

Fig. 4. Streamlines for various heating chip positions at three different Ra values.

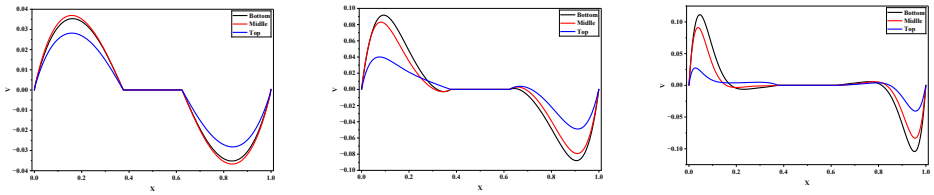

Fig. 5. Variation of the vertical velocity component along the enclosure mid-plane for $\phi = 0.06$

Table 4. Nu_{av} for different chip positions and different Ra.

	Left Bottom	Left middle	Left top
Ra = $\mathbf{10^3}$	0.9045	0.990	0.771
Ra = $\mathbf{5.10^4}$	3.216	3.364	2.249
Ra = $\mathbf{10^6}$	7.665	7.780	5.266

Conclusion

The present investigation numerically examines natural convection heat transfer in a square cavity filled with a Fe_3O_4-Al_2O_3/water hybrid nanofluid using the LBM. The study mainly aims to assess how the heating chip location and governing parameters, particularly the Rayleigh number, influence the thermal performance of the system. Analysis of the flow lines shows that the chip placed in the left midlle position generates the most organized and efficient flow. The average Nusselt values confirm that this position optimizes heat transfer to the cold wall. Overall, the combination of a high Rayleigh number and a centrally located chip maximizes the thermal performance of the cavity, promoting intense thermal gradients and optimal fluid circulation.

Reference

[1] M. Qaffou, Y. Ighris, Z. Abbassi, Y. Elguennouni, M. Hssikou, and J. Baliti, "Natural Air Convection Using LBM in a Cavity Heated Linearly," *Defect Diffus. Forum*, vol. 449, pp. 47–58, 2026, doi: 10.4028/p-2PJyYJ.

[2] I. Umar Ibrahim, M. Sharifpur, and J. P. Meyer, "Mixed Convection Heat Transfer Characteristics of Al2O3 – MWCNT Hybrid Nanofluid under Thermally Developing Flow; Effects of Particles Percentage Weight Composition," *Appl. Therm. Eng.*, vol. 249, 2024, doi: 10.1016/j.applthermaleng.2024.123372.

[3] Y. Ighris, B. El hadoui, J. Baliti, Y. Elguennouni, and M. Hssikou, "Optimizing thermal management of convective heat transfer in a complex nanofluid-filled cavity using the lattice Boltzmann method," *Int. J. Numer. Methods Heat Fluid Flow*, vol. 35, no. 5, pp. 1845–1883, Jun. 2025, doi: 10.1108/HFF-01-2025-0044.

[4] M. Qaffou *et al.*, "Analysis of Natural Convection Using the Lattice Boltzmann Method (LBM)," *Eng. Mater.*, vol. Part F1447, pp. 1–11, 2026, doi: 10.1007/978-3-032-15481-1_1.

[5] P. Rajarajeswari *et al.*, "Finite Element Numerical Simulation of Free Convection

Heat Transfer in a Square Cavity Containing an Inclined Prismatic Obstacle With Machine Learning Optimization," *Heat Transf.*, vol. 54, no. 4, pp. 2675–2690, 2025, doi: 10.1002/htj.23315.

[6] F. Garoosi, F. Hoseininejad, and M. M. Rashidi, "Numerical study of natural convection heat transfer in a heat exchanger filled with nanofluids," *Energy*, vol. 109, pp. 664–678, Aug. 2016, doi: 10.1016/j.energy.2016.05.051.

[7] B. M. Al-Srayyih *et al.*, "Simulation investigation of the oscillatory motion of two elliptic obstacles located within a quarter-circle cavity filled with Cu-Al2O3/water hybrid nanofluid," *Numer. Heat Transf. Part A Appl.*, vol. 86, no. 5, pp. 1328–1352, 2025, doi: 10.1080/10407782.2023.2279248.

[8] F. Ouallal, A. Hakim, and S. Raghay, "A numerical study for viscoelastic fluid flow around obstacles embedded inside a square cavity: A lattice Boltzmann approach," *J. Phys. Conf. Ser.*, vol. 3027, no. 1, 2025, doi: 10.1088/1742-6596/3027/1/012054.

[9] Y. Ighris, M. Qaffou, J. Baliti, Y. Elguennouni, and M. Hssikou, "Thermal management optimization of natural convection in a triangular chamber: Role of heating positions and ternary hybrid nanofluid," *Phys. Fluids*, vol. 36, no. 9, 2024, doi: 10.1063/5.0226427.

[10] M. Izadi, R. Mohebbi, D. Karimi, and M. A. Sheremet, "Numerical simulation of natural convection heat transfer inside a ⊥ shaped cavity filled by a MWCNT-Fe3O4/water hybrid nanofluids using LBM," *Chem. Eng. Process. - Process Intensif.*, vol. 125, pp. 56–66, Mar. 2018, doi: 10.1016/j.cep.2018.01.004.

[11] Y. Ighris, B. El hadoui, M. Qaffou, J. Baliti, Y. Elguennouni, and M. Hssikou, "Hybrid lattice Boltzmann modeling of magneto-convection in Fe2O3/MWCNT ferro-nanofluid for thermal management applications," *Int. J. Therm. Sci.*, vol. 220, 2026, doi: 10.1016/j.ijthermalsci.2025.110433.

[12] B. Ghasemi, S. M. Aminossadati, and A. Raisi, "Magnetic field effect on natural convection in a nanofluid-filled square enclosure," *Int. J. Therm. Sci.*, vol. 50, no. 9, pp. 1748–1756, 2011, doi: 10.1016/j.ijthermalsci.2011.04.010.

[13] R. J. Krane and J. Jessee, "Some Detailed Field Measurements for a Natural Convection Flow in a Vertical Square Enclosure.," vol. 1, pp. 323–329, 1983.